BNL-111993-2016-TECH
C-A/AP/560;BNL-111993-2015-IR

On the image of AGS 3He2+ no in the blue

F. Meot

September 2015

Collider Accelerator Department
Brookhaven National Laboratory

U.S. Department of Energy
USDOE Office of Science (SC), Nuclear Physics (NP) (SC-26)

DISCLAIMER

BNL-111993-2015-IR

C-A/AP/560
September 2015

On the Image of AGS $^3He^{2+}$ $\vec{n}_0$, in the Blue

F. Méot, H. Huang, N. Tsoupas

Collider-Accelerator
Department Brookhaven
National Laboratory Upton, NY
11973

U.S. Department of Energy
Office of Science, Office of Nuclear Physics

On the Image of AGS $^3\mathrm{He}^{2+}$ $\vec{n}_0$, in the Blue

F. Méot, H. Huang, N. Tsoupas

BNL C-AD, Upton, LI, NY 11973

March 2016

Abstract

This note addresses the transport of Helion spin $\vec{n}_0$ vector, from its periodic orientation in the AGS to RHIC Blue ring injection kicker, via the AGS extraction system and the AtR line. The goal is to investigate optimal injection energy into RHIC, in the matter of Helion spin matching, in the hypothesis of equal warm and cold snake strengths in the AGS.

The study uses recently computed OPERA 3-D field maps of the AGS cold snake, including possibility of independent solenoid and helix settings (as discussed in Tech. Note C-A/AP/485), together with the machinery of the AGS and AtR models developed in the stepwise ray-tracing code Zgoubi.

Computing tools and methods employed are discussed as well, in order to facilitate possible further checks or investigations. They are however similar to those used in an earlier study regarding the image in RHIC Blue and Yellow of AGS $\vec{n}_0$ via the AtR in the case of proton beam (Tech. Note C-A/AP/502), which can be referred to for additional details.

Tech. Note C-A/AP/560

Contents

1 Introduction

In preparation of RHIC/eRHIC plans concerning polarized Helion beams ($^3He^{2+}$ stored in Blue), the question arises of the optimum extraction energy from the AGS with regard to the transport of the spin $\vec{n}_0$ vector, via the non-planar AtR line [1], Fig. 1, from its periodic, non fully vertical, orientation at G10 extraction kicker in the AGS, to the downstream end of RHIC Blue ring injection kicker where it is expected to be as close as possible [2] to the periodic, vertical, RHIC $\vec{n}_0$. As a matter of fact, due to the interleaved horizontal and vertical bends in the AtR, the image of the AGS $\vec{n}_0$ at RHIC injection point varies with beam energy.

Quasi-equal warm and cold snake strengths, $14 \sim 15\%$, are considered here [3], meaning in particular lower cold snake field compared to polarized proton operation so reducing optics perturbation at low energy. This study leans on recent work regarding the AGS snake field maps [1], and on earlier similar study regarding polarized proton beams [2].

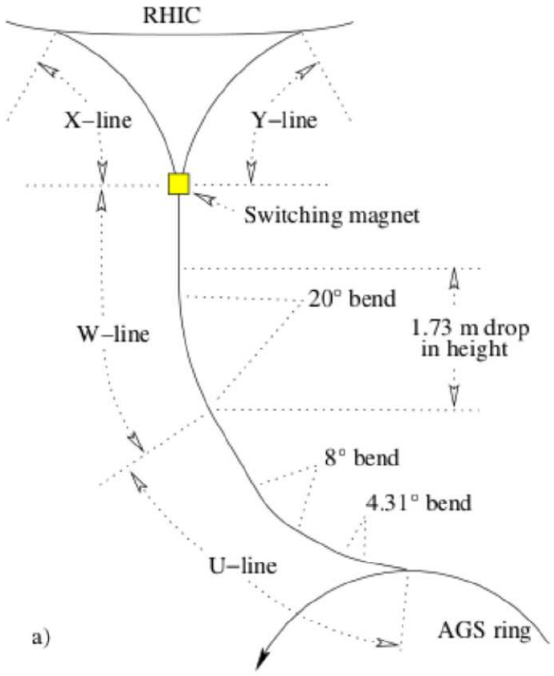

Figure 1: The AtR line.

Details regarding the AGS to RHIC transport line, geometry, spin considerations, coordinate system, etc., can be found in Ref. [3]. A treatment of the AGS to RHIC spin matching can be found in an earlier works, Refs. [4, 5]. On the other hand, in order to allow answering possible questions regarding details of the geometry and optics of the AGS and AtR models in Zgoubi [2, 6, 7], and also in order to facilitate further checks or investigations, the Zgoubi I/O data files relating to the present work have been archived in dedicated folders in

$$/rap/lattice\_tools/zgoubi/AgsZgoubiModel/AtR/3He/n0$$

They can be run using the Zgoubi executable available on-line. Various aspects of the computing tools and methods employed in the present study will be discussed in due place in the sequel in that aim.

The present investigations are based on separate 3-D OPERA maps of the AGS cold snake solenoid and helix [1]. These OPERA field maps of the cold snake are archived in

$$/rap/lattice\_tools/zgoubi/AgsZgoubiModel/snakeFieldMaps/coldSnake/RGFiles$$

[1] AGS and RHIC planes differ in height by 1.73 m.

[2] Due to the partial snakes in the AGS and to the vertical bends in the AtR, spin matching from AGS to RHIC can not be perfect.

[3] By contrast with polarized proton beams for which the two snakes have non-equal strengths, respectively 6% (warm snake) and 11%(cold snake).

The warm snake OPERA maps are archived in

$$/rap/lattice\_tools/zgoubi/AgsZgoubiModel/snakeFieldMaps/warmSnake/$$

Users can find guidance in the "README" files included in these folders.

Table 1: Characteristics of the warm and cold snakes. ($|G\gamma|$: $7.5 \rightarrow 60$ corresponds to $B\rho$: $6.968 \rightarrow 67.00$ T.m). Reference system in the magnets : x longitudinal, y radial, z vertical.

		Warm snake$^{(a)}$	**Cold snake**$^{(c)}$
		set/meas./OP$^{(b)}$	
Helix coil current	A	2670/2635/2540	189
(relative to 350 Amp)	*%*	-	*(54)*
Solenoid current	A	-	80
(relative to 350 Amp)	*%*	-	*(22.8)*
Snake strength, $\|G\gamma\|$: $7.5 \rightarrow 60$	%	$20 \rightarrow 14$	$19.5 \rightarrow 15$
$\|\vec{B}\|$ at magnet center, B_{00}	T	1.5309	1.704 (helix+sol)
$\int_{\text{axis}} \|\vec{B}(x)\|\, dx$	T.m	3.2276	3.402
Straight mag. $\mathcal{L} = \frac{\int_{\text{axis}} \|\vec{B}\|\, dx}{B_{00}}$	m	2.108	1.997
For $\|G\gamma\|$: $7.5 \rightarrow 60$ **:**			
Max. $\|\vec{B}(s)\|$ on orbits	T	$1.5333 \rightarrow 1.5309$	$1.691 \rightarrow 1.694$
$\int_{\text{orbit}} B_z(s)\, ds$	T.m	$-0.16 \rightarrow -0.017$	$-0 \rightarrow +0.12$
Orbit radius	mm	$19 \rightarrow 1.9$	$18.2 \rightarrow 1.9$
Spin prec. ϕ	deg	$35.6 \rightarrow 25.25$	$35 \rightarrow 26.8$

(a) Field map named "table55.tab" was used in Zgoubi input data files.
(b) Case 2670 A : current set in AGS controls for 1.53 T field on plateau. Case 2635 A : measured current with the former setting. Case 2540 A : theoretical value in OPERA, using the "perfect model" of the snake (i.e., the model of the magnet free of deformation [8]) yielding 1.53 T on the plateau.
(c) A linear combination of the following two 3-D OPERA field maps was used [1] :
- ags-full-coilv5-x06-rerun2-x071-integral-x5y5z10mm/b_ags-full-coilv5-x06-rerun2-x071-integral-x5y5z10mm.table,
- ags-full-sold3-only-nodal-x5y5z10mm/b_ags-full-sold3-only-nodal-x5y5z10mm-was actually-integral.table.

2 Snake hypotheses

Equal warm and cold snake strengths, $14 \sim 15\%$, are considered. As a consequence, the field in the warm snake is the same as for protons, $B_{00} = 1.53$ T at magnet center, whereas the cold snake is operated with lower field, $B_{00} = 1.7$ T compared to $B_{00} = 2.1$ T for protons [2, 7].

General snake parameters are given in Tab. 1. Note for reference, that the lower rigidity considered in the Table is 6.968 T.m ($G\gamma$=-7.5), close to proton's 7.205 T.m injection rigidity ($G\gamma$=4.5), whereas the highest rigidity explored for $^3\text{He}^{2+}$ is $\sim$70 T.m ($G\gamma$ in -60 $\sim$ -65 region) while extraction rigidity in the case of protons is 79.4 T.m ($G\gamma$=45.5).

• **Warm snake :** The field map "table.55.map" is used. The main properties it yields are recalled in Tab. 1, col. .3 (more in Ref. [1]). Typical field along the orbit is displayed in Fig. 2.

In the vicinity of $B_{00} = 1.53$ T, $^3\text{He}^{2+}$ spin precession along the AGS cycle can be interpolated using (Fig. 3)

$$\mu(B, G\gamma)[\text{deg.}] = (B/B_{00})^2 \times \left(24.839 - 23.721/G\gamma - 133.1/(G\gamma)^2 - 4172.7/(G\gamma)^3\right) \quad (1)$$

$i.e.$ in particular, μ =25.4 to 25.2 degrees (14.1 to 14 %) in the range $|G\gamma| \in [40, 60]$ with regular field value $B = 1.53$ T.

WARM SNAKE

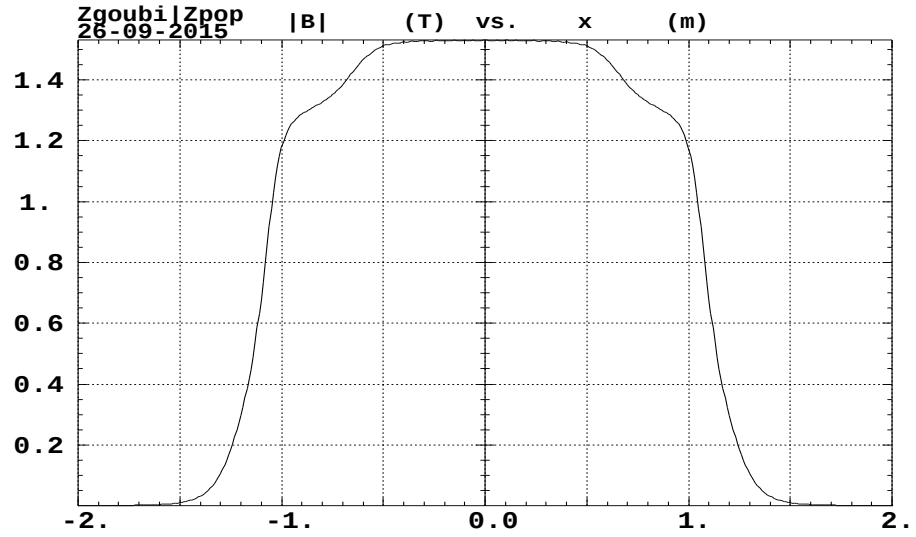

Figure 2: Total field $|B| = \sqrt{B_x^2 + B_y^2 + B_z^2}$ experienced along the helical orbit in the warm snake, at $G\gamma$=-45.5 (marginally dependent on $G\gamma$).

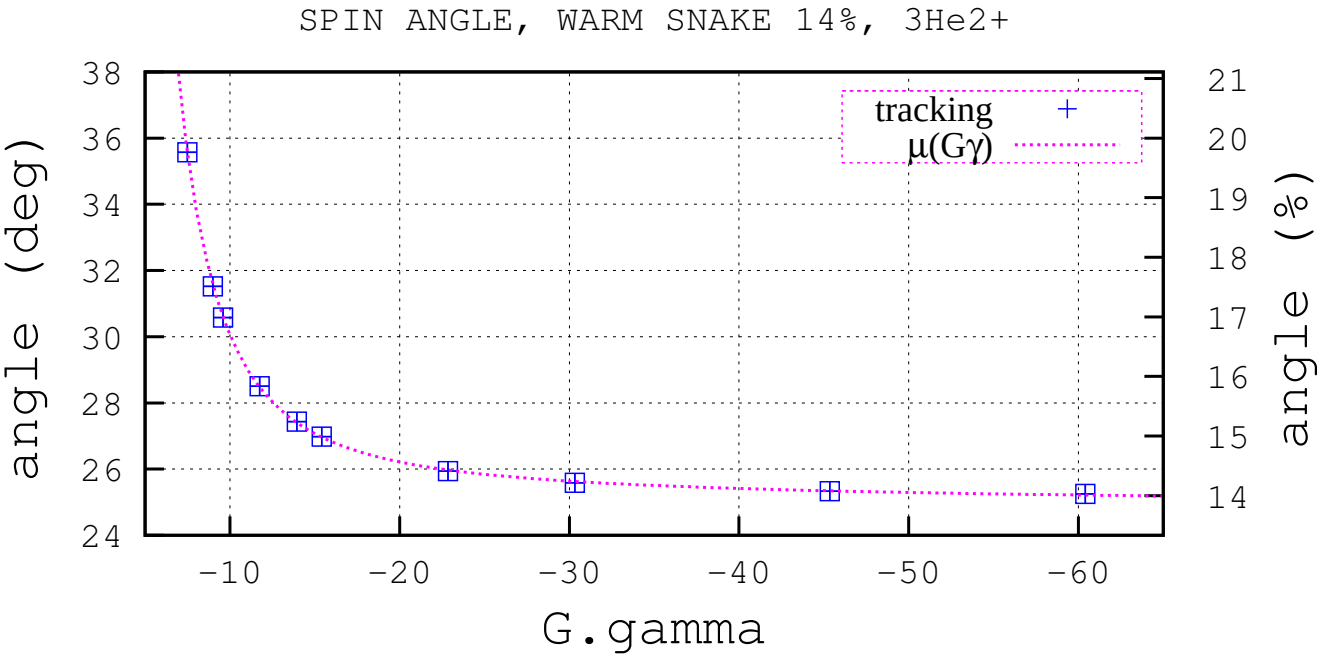

Figure 3: $G\gamma$ dependence of $^3He^{2+}$ spin precession angle in the warm snake, and interpolation function Eq. 1.

COLD SNAKE

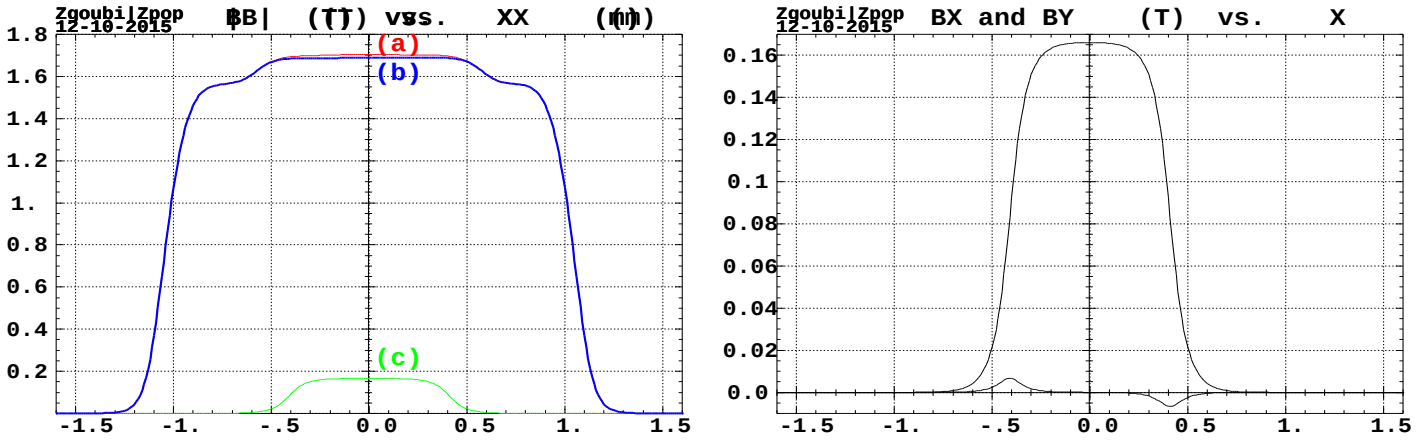

Figure 4: Left : Total field $|B| = \sqrt{B_x^2 + B_y^2 + B_z^2}$ experienced along the longitudinal axis of the cold snake. (a) Helix and solenoid both on, (b) helix field, solenoid off, (c) solenoid field, helix off. Right : Longitudinal and radial field contributions from the solenoid.

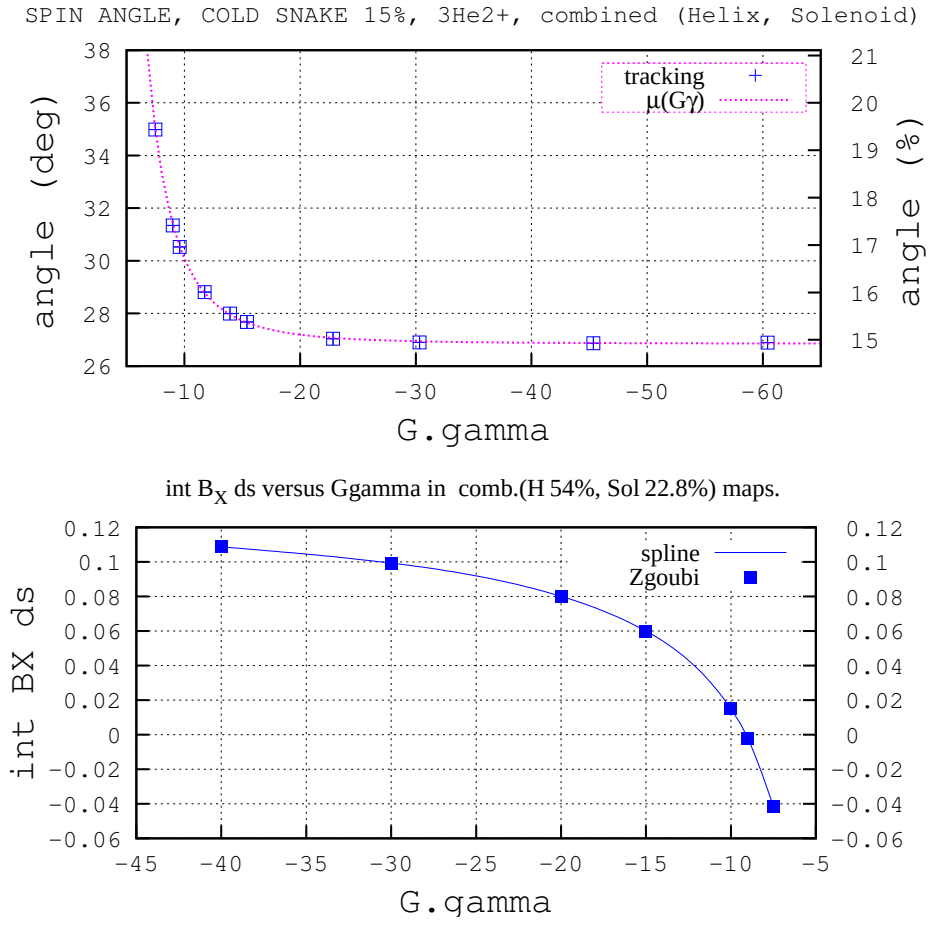

Figure 5: Top : $G\gamma$ dependence of $^3\mathrm{He}^{2+}$ spin precession angle in the cold snake, and interpolation function Eq. 2. Bottom : Integral of the longitudinal field component, $\int B_x\, ds \approx \int B_s\, ds$, canceling at about $G\gamma = -9$.

• **Cold snake :** The cold snake map is obtained by combining independent 3-D OPERA helix and solenoid field maps, as follows (*cf.* Tab. 1, and Ref. [1] for details) :

(i) the helix current is set to 54% of its 350 Amp maximum ($i.e.$, 189 Amp). However the OPERA map has been computed for 0.76×350=266 Amp, therefore it has to be scaled down to 71% in the present study,

(ii) the solenoid current is set to 22.8 % of its 350 Amp maximum (80 Amp) so to cancel the helix induced $\int B_s\, ds$ at $G\gamma = -9$.

In the matter of Zgoubi input data, this combination thus takes the form

1.016 × [0.76 × ags-full-coilv5-x06-rerun2-x071-integral-x5y5z10mm/b_ags-full-coilv5-x06-rerun2-x071-integral-x5y5z10mm.table,
⊕ 0.228 × ags-full-sold3-only-nodal-x5y5z10mm/b_ags-full-sold3-only-nodal-x5y5z10mm-was actually-integral.table.]

with the front coefficient "1.016" an empirical value that ensures same spin precession as would a complete, single, helix+solenoid OPERA computation map, this is discussed in Ref. [1].

With this combination one gets the following (Fig. 4) :

(i) at center of the snake, along the magnet axis, the helix field is $B_{00} = 1.70$ T, the solenoid field is $B_{\rm Solenoid} = 0.166$ T,

(ii) cancellation of coupling at $G\gamma = -9$. If $B_{\rm Helix}$ is changed, then $B_{\rm Solenoid}$ should be scaled as $B^2_{\rm Helix}$ [1].

In the vicinity of $B_{00} = 1.7$ T, the spin precession along the AGS cycle can be interpolated using (Fig. 5)

$$\mu(B, G\gamma)[\text{deg.}] = (B/B_{00})^2 \times \left(26.831 - 2.672/(G\gamma) - 114.96/(G\gamma)^2 - 4144/(G\gamma)^3\right) \quad (2)$$

$i.e.$ in particular, μ =26.8 degrees (14.9%) in the range $|G\gamma| \in [-60, -40]$ for field value $B = 1.7$ T.

3 OCO in the AGS with G09 and H11 bumps

Zgoubi input and output data files for this OCO study can be found in

$$/rap/lattice\_tools/zgoubi/AgsZgoubiModel/AtR/3He$$

Note : Coordinate system used in these dynamics simulations :

x radial, y vertical, s along trajectory

AGS has been tuned to regular extraction optics conditions, see Tab. 2 (orbit constraints can be found in App. A.1, optical functions are displayed in Fig. 17, App. A).

Local compensation of dipole defect at the snakes is not needed (by contrast with proton simulations [2]) due to the lower cold snake field (residual horizontal and vertical orbits in $\sim \pm 0.1$ mm $\sim \pm 0.6$ mm range respectively, Fig. 6). Note that the $x = 0$ axis in Fig. 6 and following ones, defines the bare AGS OCO, bump and other orbit excursions in the following are given with respect to that axis.

The optical setting includes the superimposed "G09" and "H11" extraction bumps, as displayed in Fig. 7. "G09" positions the orbit at G10 kicker, "H11" positions the orbit at H10 extraction septum, on the machine side of the septum. "G09" and "H11" bumps are horizontally well closed by using an independent power supply for each one of the six dipole back-leg windings in each bump (respectively, F08CD, F09BF, G02BF, G03CD, G16AD, G17CF for G09 and H04CD, H05AF, H18CF, H19BD, I12BD, I13CF for H11). Note that in real life only two power supplies are used, one per series, so yielding some residual horizontal orbit.

Changes in the orientation of the local $\vec{n}_0$ at the extraction septum H10, due to the residual orbit, are expected to be marginal.

Table 2: Typical AGS parameters in Zgoubi for search of periodic and extracted $\vec{\mathbf{n}}_{\mathbf{0}}$.

γG		-40 to -60
Rigidity	(T.m)	44.5 to 67
Closed orbit length	(m)	807.5
Qx, Qy		[8].75, [8].78
Q'x, Q'y		-2.5, 2.5
Periodic parameters (G10 off) :		
- At middle of "G10" kicker :		
x_{co}, x'_{co}	(mm, mrad)	-61, +5.5
D_x, D'_x	(m,-)	-2.3, 0.11
- At middle of "H10" :		
x_{co}, x'_{co}	(mm, mrad)	-48, +3.7
$\beta_x,\ \beta_y$	(m)	7, 26
$\alpha_x,\ \alpha_y$		+0.8, -2
D_x, D'_x	(m,-)	-1.7, -0.02
Orbit coordinates at "H10", G10 on :		
x_{co}, x'_{co}	(mm, mrad)	-75.5, +5.8

4 Periodic and extracted $\vec{n}_0$ at H10

Snake settings considered in the following are as described in Sec. 2, $14 \sim 15\%$ strength, spin rotation angle as displayed in Fig. 3 (warm snake) and Fig. 5 (cold snake). The orbit is as discussed in the previous section (Figs. 6, 7).

Finding $\vec{n}_0$: The "FIT" procedure in Zgoubi is used to find the local $\vec{n}_0$ on the closed orbit. Appendix B gives excerpts of the AGS sequence and the 'FIT' instructions for closed orbit and $\vec{n}_0$ search[4]. As an example Fig. 8 displays the vertical projection of $\vec{n}_0$ along the AGS ring, at half-integer $G\gamma$ values in the interval $[-59.5, -40.5]$, S_y values in the A and F-L superperiods switch between $S_y \sim 1$ and $S_y \sim 0.925$ as observed as well in Fig. 9-top.

In a second stage G10 is switched on, so displacing the orbit in the G10 - H10 region and ending up with the expected 7.55 cm beam off-centering at H10 for extraction [4] (Fig. 7). That periodic $\vec{n}_0$ at G10 is the quantity which is transported along the AtR down to RHIC kicker.

The results of the $G\gamma$ scan are displayed in Fig. 9. The penalty reached by the FIT procedure is displayed (along with S_y graph) to check the convergence of the FIT on closed orbit and periodic $\vec{n}_0$.

[4]The orbit is close to zero as discussed earlier, therefore orbit constraints are of little effect on $\vec{n}_0$.However, such would not be the case with stronger snakes, or non-fully closed G09 and H11 bumps.

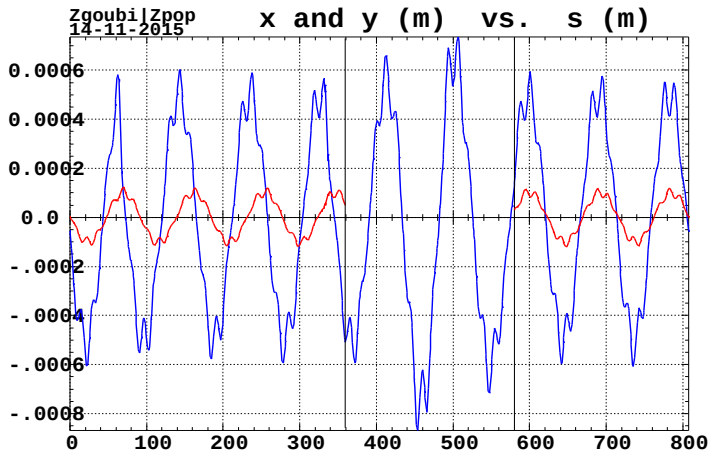

Figure 6: Residual horizontal (red) and vertical (blue) orbit excursions in the present simulation conditions, with G09 and H11 bumps set (the x orbit in the G09 and H11 region between the vertical lines ($360 \sim 580$ m region) has been removed, details shown in Fig. 7). AGS settings are as in Tab. 2, both snakes are on, $14 \sim 15\%$ strength. The vertical orbit is induced by the snakes.

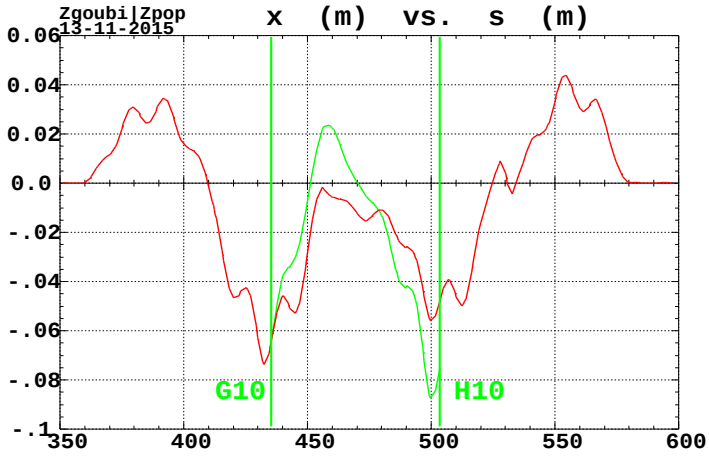

Figure 7: Horizontal orbit excursion in G10 kicker and H10 septum regions, with G09 and H11 bumps tuned for extraction. AGS settings are as in Tab. 2, G10 kicker is either off (periodic orbit, red) or on (extracted path from G10 to H10, green).

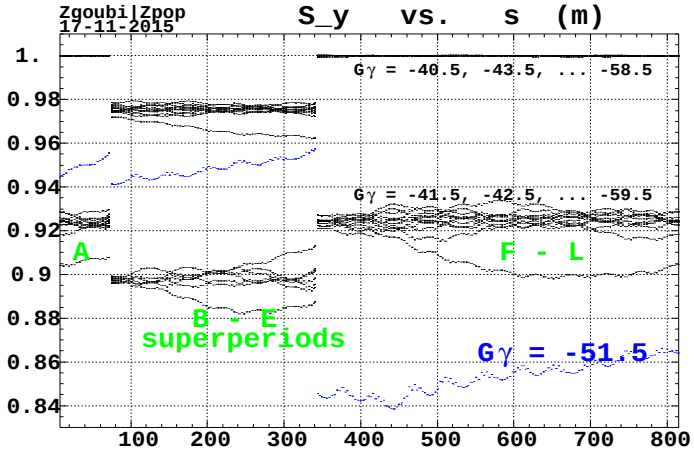

Figure 8: Vertical component of periodic $\vec{n}_0$ along AGS for $^3\mathrm{He}^{2+}$, at $G\gamma = \mathrm{n} - \frac{1}{2}$, integer $n \in [-59, -40]$. $\vec{n}_0$ is not closed in the case $G\gamma = -51.5$ (blue), $i.e.$, next to the strong $G\gamma = -5 \times P + Q_y$ resonance (P=12 superperiods), this is due to the sensitivity to accuracy on initial orbit coordinates (which are non-zero, due to the snakes).

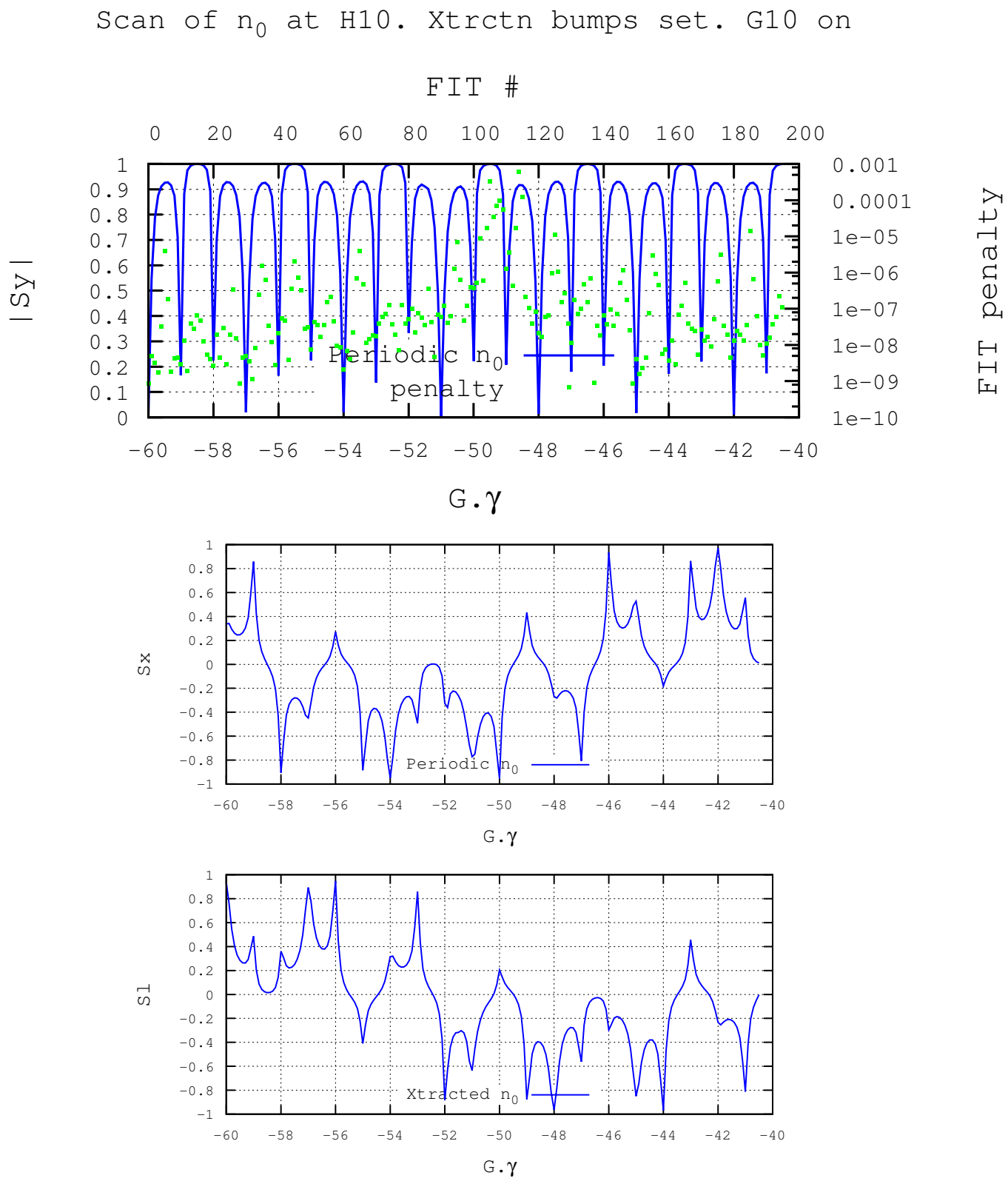

Figure 9: $\vec{n}_0$ components at H10 septum in the range $G\gamma \in [-60, -40]$. The top plot also displays the penalty value reached by the fitting procedure (upper horizontal scale and right vertical scale).

5 $\vec{n}_0$ transmission, from H10 to RHIC Blue kicker

5.1 AtR

Zgoubi model : A model of the AtR line in Zgoubi has been obtained by translation from MAD8 data files. It covers from UBEGIN to RHIC kicker (Fig. 1),

- then H10 septum is added,

- as well as H11, H12 and H13 AGS main magnet wakes, which the extracted path downstream of the septum does cross. They are simulated in a simplified way that takes care simply of the orbit, namely, with reduced-field H11BD (11.85 mrad), H12BD (6.18 mrad), H13CF (3.67 mrad).

The AtR (Fig. 1) is organized as follows :

- the UBEGIN to W-End section is common to both Blue and Yellow injections,

- then the "switching magnet" directs the beam towards the X (RHIC-Blue) branch.

- The X and Y lines differ essentially by the sign of the angle in the bends, and by the particular settings of the injection path along RHIC arcs. We are only interested in the X branch since $^3\mathrm{He}^{2+}$ will go to the Blue.

That model of the AtR in Zgoubi, as well as the various files used for checking transport matrices against MAD8, checking the orbits along the AtR, etc., have been archived in

$$/rap/lattice\_tools/zgoubi/AgsZgoubiModel/AtR/3He/n0$$

The optics of the U-W-X transport as obtained from Zgoubi is given in Fig. 10.

Additional informations regarding general AtR geometrical data can be found in Ref. [3].

• **Transport matrices, from H10 to RHIC Blue kicker :** The end-to-end transport matrix from both MAD8 and Zgoubi is displayed below for cross-check. The non-zero anti-diagonal blocks arise from the presence of skew optics along the line, in relation with RHIC ring being at lower elevation than AGS.

From H10 to RHIC-Blue kicker :

```
MAD8

   Length: 581.026
      -2.796068       17.367812       -0.016389       -0.033368        0.000000       -1.065488
      -0.039314       -0.113439       -0.000903       -0.003215        0.000000       -0.024004
       0.010052       -0.107989        1.184843       10.183856        0.000000        0.020349
       0.000160        0.000523       -0.168178       -0.601530        0.000000        0.003584
      -0.025262        0.538168       -0.007100       -0.046116        1.000000       -2.822765
       0.000000        0.000000        0.000000        0.000000        0.000000        1.000000

ZGOUBI

   length :   581.02556
      -2.78658         17.2839       -1.637868E-02   -3.346093E-02     0.00000        -1.06058
     -3.943741E-02   -0.114243       -9.066873E-04   -3.230374E-03     0.00000       -2.423199E-02
      1.007545E-02   -0.108164         1.18162         10.1841         0.00000        2.033039E-02
      1.593392E-04    5.295908E-04   -0.167967       -0.601396         0.00000        3.588438E-03
      2.573239E-02   -0.540403        7.090202E-03    4.615573E-02     1.00000         2.82454
       0.00000         0.00000         0.00000         0.00000         0.00000         1.00000
```

• **Optical functions at UBegin, in MAD AtR model :**

```
-------------------------------------------------------------------------------------------------------------------------------
     ELEMENT SEQUENCE       I              H O R I Z O N T A L              I              V E R T I C A L
pos.  element occ.     dist I   betax  alfax   mux    x(co)  px(co) Dx    Dpx  I   betay  alfay   muy    y(co)  py(co) Dy    Dpy
no.   name    no.      [m]  I   [m]    [1]     [2pi]  [mm]   [.001] [m]   [1]  I   [m]    [1]     [2pi]  [mm]   [.001] [m]   [1]
-------------------------------------------------------------------------------------------------------------------------------
begin U          1     0.000   37.500 -4.100   0.000  0.000  0.000 -1.500-0.130    6.500  0.850   0.000  0.000  0.000  0.000 0.000
    1 UBEGIN     1     0.000   37.500 -4.100   0.000  0.000  0.000 -1.500-0.130    6.500  0.850   0.000  0.000  0.000  0.000 0.000
-------------------------------------------------------------------------------------------------------------------------------
```

This is the starting values (at s=0) in Fig. 10, and as well the values used in Sec. 6.3.

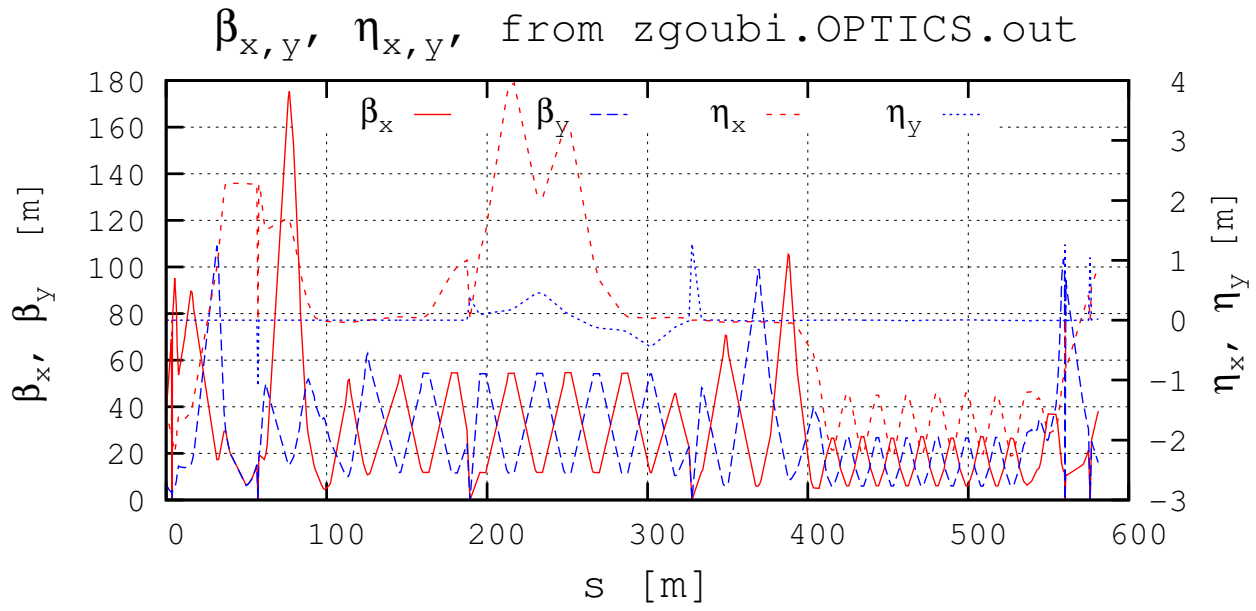

Figure 10: The optics of the U-W-X transport as obtained from Zgoubi. (Discontinuities observed at some locations are artifacts - local change of frame.) The values of the optical functions at UBegin (s=0 on the figure), are given in page 11.

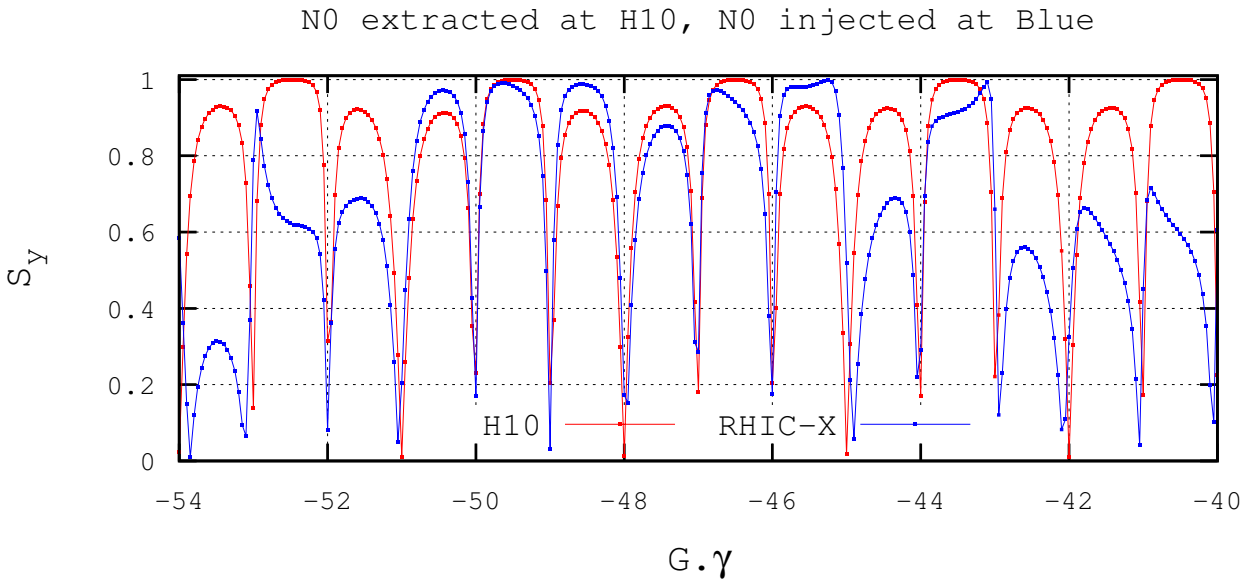

Figure 11: Vertical component of the spin vector $\vec{n}_0$ at extraction from AGS (at H10 septum, red curve) and at RHIC Blue injection kicker (blue curve). The markers show the computed values, the line in between is to guide the eye.

• Values of the spin $\vec{n}_0$ vector components at H10 septum (cols. 1-3, first line of two) and at RHIC Blue injection kicker (second line), for half-integer values of $G\gamma$ taken between -40.5 and -52.5 (rightmost column).

S_l	S_x	S_y	gamma	G.gamma	
7.4116E-03	-1.0685E-02	-9.9991E-01	9.67937	-40.500	at H10 septum
8.0409E-01	9.7770E-03	-5.9442E-01			at RHIC Blue kicker
-9.8257E-02	3.7021E-01	-9.2373E-01	9.91837	-41.500	at H10 septum
6.2954E-01	-5.0819E-01	-5.8772E-01			at RHIC Blue kicker
-3.2303E-01	2.0877E-01	9.2307E-01	1.0157E+01	-42.500	at H10 septum
7.3667E-01	3.9973E-01	5.4545E-01			at RHIC Blue kicker
3.5675E-03	-1.4856E-02	9.9988E-01	1.0396E+01	-43.500	at H10 septum
2.6516E-01	-3.0370E-01	9.1512E-01			at RHIC Blue kicker
1.8437E-01	3.4241E-01	9.2127E-01	1.0635E+01	-44.500	at H10 septum
-7.0689E-01	-2.5295E-01	6.6054E-01			at RHIC Blue kicker
1.1205E-01	-3.6081E-01	9.2588E-01	1.0874E+01	-45.500	at H10 septum
-8.1156E-02	1.5480E-01	9.8460E-01			at RHIC Blue kicker
1.4836E-02	2.0876E-02	9.9967E-01	1.1113E+01	-46.500	at H10 septum
-8.8845E-02	3.2286E-01	9.4226E-01			at RHIC Blue kicker
-3.5932E-01	-1.2062E-01	9.2538E-01	1.1352E+01	-47.500	at H10 septum
-3.9527E-01	2.9198E-01	8.7091E-01			at RHIC Blue kicker
-1.7621E-01	-3.4857E-01	-9.2056E-01	1.1591E+01	-48.500	at H10 septum
-1.0990E-01	1.0941E-01	-9.8790E-01			at RHIC Blue kicker
4.8253E-03	-7.0869E-03	-9.9996E-01	1.1830E+01	-49.500	at H10 septum
-4.7719E-02	-1.6986E-01	-9.8431E-01			at RHIC Blue kicker
-3.6751E-01	1.1499E-01	-9.2287E-01	1.2069E+01	-50.500	at H10 septum
1.8401E-01	-1.1128E-01	-9.7660E-01			at RHIC Blue kicker
3.5720E-01	1.0366E-01	-9.2825E-01	1.2308E+01	-51.500	at H10 septum
4.0407E-01	6.0138E-01	-6.8924E-01			at RHIC Blue kicker
1.3267E-02	2.5562E-02	-9.9958E-01	1.2547E+01	-52.500	at H10 septum
6.5645E-01	-4.1795E-01	-6.2799E-01			at RHIC Blue kicker

5.2 $G\gamma$ scan

The optics settings and the orbits are as discussed in the previous sections, including
- "G09 bump" (at extraction kicker) and "H11 bump" (at H10 septum),
- G10 kicker off when determining the periodic $\vec{n}_0$ in the AGS,
- orbit deviation by G10 kicker when determining $\vec{n}_0$ at the start of the AtR line,
- dipole effect of the wakes at the H10, H11 and H13 AGS main magnets.

A scan of $G\gamma$ in the range $[-54, -40]$ yields Fig. 11 which shows the vertical projection of the $\vec{n}_0$ vector at two different locations : at H10 septum in the AGS after extraction by G10 kicker and at RHIC-Blue kicker. The optimum extraction $G\gamma$ can be determined from the scan : it has to be close to a half-integer value, and such that the vertical projection of the $\vec{n}_0$ is closest to 1 at the injection kicker at the downstream end of the X line. Detailed numerical values of $\vec{n}_0$ components at H10 and at RHIC kicker, for half-integer $G\gamma$ in $[-52.5, -40.5]$, are given on page 13.

6 Perturbations

We now include some perturbations on initial beam conditions, and check their effect on the spin precession vector.

6.1 $\vec{n}_\delta$ transmission to RHIC Blue kicker

In order to evaluate the effect of momentum spread on the dispersion of the spin precession vector orientation at RHIC kicker, a $G\gamma$ scan is now performed considering instead chromatic orbits in the AGS, $i.e.$, closed orbits that differ from the AGS OCO (the AGS "Optimum Closed Orbit" is the closed orbit for a particle with reference momentum p_0, corresponding to the main magnet settings) due to a (relative) difference in momentum $\delta \equiv \delta p/p = (p - p_0)/p_0$. To first order a chromatic orbit is defined by, at all s and with respect to the OCO,

$$x(s) = D_x(s) \times \delta, \;\; x'(s) = D'_x(s) \times \delta, \;\; y(s) = D_y(s) \times \delta, \;\; y'(s) = D'_y(s) \times \delta$$

with $D_{x,y}$, $D'_{x,y}$ the periodic dispersion and its derivative taken on the OCO, and the vertical amplitude actually negligible since $D_y(s)$ and $D'_y(s)$ (induced by the snakes) are small (Fig. 17, page 19)

Apart from being performed for a non-zero δ value, the algorithm for this $G\gamma$ scan is otherwise the same as discussed/used in the previous sections, namely :

- first, the chromatic orbit in the AGS is determined,
- then the periodic spin precession vector $\vec{n}_\delta$ on that orbit is computed,
- its periodic value at G10 is transported to the AtR side of H10 septum ($i.e.$, G10 kicker switched on),
- from there $\vec{n}_\delta$ is transported along the AtR line to RHIC Blue kicker.

The AGS main magnets are set for $G\gamma = -n - \frac{1}{2}$ with $n \in [45, 49]$ integer (the vertical bars), whereas AGS's $\vec{n}_\delta$ is found for eight off-momentum values $\delta = \pm 2\,10^{-3}, \pm 1.5\,10^{-3}, \pm\,10^{-3}, \pm 0.5\,10^{-3}$ around each of these magnet settings, and then transported to RHIC kicker.

Note that the position of the extracted chromatic orbit at H10 is

$$x_\delta = x_{co} + D_x \times \delta, \qquad x'_\delta = x'_{co} + D_x \times \delta$$

with (values from Tab. 2) $x_{co} = -75.5$ mm, $x'_{co} = +5.8$ mrad, $D_x = -1.7$ m, $D'_x \approx 0$.

Details of the off-momentum orbits over the δ range explored are shown in Fig. 12. Along the AGS the chromatic closed orbit x-excursion is in a few mm range (of the order of $D_x \times \delta$), y-excursion in mm range. At

the downstream end of the X line $\Delta x \approx \pm 3$ mm, while the chromaticity induced y-excursion is quasi-zero. These (essentially horizontal) orbit excursions are considered small enough, compatible with the present investigation on $\vec{n}_\delta$ given the results regarding the latter, as follows.

The vertical component of the chromatic spin vector $\vec{n}_\delta$ in this off-momentum $G\gamma$ scan, at AGS H10 extraction septum and at RHIC Blue injection kicker locations, is displayed in Fig. 13. On-momentum $\vec{n}_0$ vertical projection (Fig. 11) is superimposed for comparison. It can be observed that $\vec{n}_0$ and $\vec{n}_\delta$ projections differ only weakly (and essentially in $G\gamma = -47.5$ region), meaning in particular that, whatever $G\gamma$ and δ, the non-zero orbit in the $\vec{n}_\delta$ case (Fig. 12) is of little influence on spin motion.

6.2 Orbit mis-positioning at AtR entrance

In this exercise, the on-momentum orbit and $\vec{n}_0$ at H10 septum are taken as they come out of the $G\gamma$ scan discussed in Sec. 5. Namely, the orbit at H10 septum is (-75.5 mm, +5.8 mrad) (Tab. 2), whereas $\vec{n}_0$ is as displayed in Fig. 9. However, prior to launching the beam into the AtR line, its initial centroid coordinates are changed, as follows :

- $x_0 = -75.5 \pm 3, \pm 6, \pm 9$ mm while $x'_0 = +5.8$ mrad (0.3325 deg) and $y_0 = 0$,
- $x'_0 = 0.3325 \pm 0.02, \pm 0.04, \pm 0.06$ degree while $x_0 = -75.5$ mm and $y_0 = 0$,
- $y_0 = -1 \rightarrow +1\,\mathrm{mm},\ \mathrm{step}\ 0.2$ mm while $x_0 = -75.5$ mm and $x'_0 = +5.8$ mrad.

The resulting perturbed beam paths along the AtR are displayed in, respectively, Fig. 12-top/right, -bottom/left, -bottom/right. The corresponding vertical projections of $\vec{n}_0$ at RHIC Blue kicker are displayed in the three homologue plots in Fig. 13.

From these data one gets the following results : compared to the unperturbed case (Fig. 11), and in the range $-50 < G\gamma < -40$,

- an horizontal orbit position perturbation $|\Delta x_0| \leq 8$ mm at H10 causes a variation $\Delta S_y < 9.5\,10^{-3}$ at RHIC kicker,
- an horizontal orbit angle perturbation $|\Delta x'_0| \leq 10$ mrad at H10 causes a variation $\Delta S_y < 5.4\,10^{-3}$ at RHIC kicker,
- a vertical orbit position perturbation $|\Delta y_0| \leq 1$ mm at H10 causes a variation ΔS_y in a 0.01-0.05 (1% to 5% absolute) at RHIC kicker.

6.3 Non-zero vertical emittance

The effect of non-zero vertical emittance is computed using a self-consistent zgoubi input data file which can be found at

$$/rap/lattice\_tools/zgoubi/AgsZgoubiModel/AtR/3He/n0/usingTOSCAMaps/emittance/$$

The method is the following :

(i) a $G\gamma$ value is considered, taken at half-integer value in the interval $[-54, -40]$,

(ii) for that $G\gamma$ value, first the periodic spin vector $\vec{n}_0$ at entrance of A01BF is computed (the choice of this origin is arbitrary, A01BF happens to be the origin of the AGS in Zgoubi), using a "fit" technique,

(iii) $\vec{n}_0$ is then transported along the orbit down to the entrance to the U line (UBegin).

(iv) At UBegin, a 500 particle bunch is then formed, with particles taken at random in a Gaussian distribution with rms value ϵ_y/π truncated at $9\sigma_{\epsilon_y}$ and with phase space beam parameters identifying with the local optical parameters at UBegin ($i.e.$, at s=0 in Fig. 10, values in page 11),
whereas, all these particles are given the same spin orientation, namely, the value of $\vec{n}_0$ obtained via (i)-(iii)

(v) that bunch is then transported along the AtR down to the Blue kicker,

(vi) back to (i) above, the interval $[-54, -40]$ is scanned for all half-integer $G\gamma$ values.

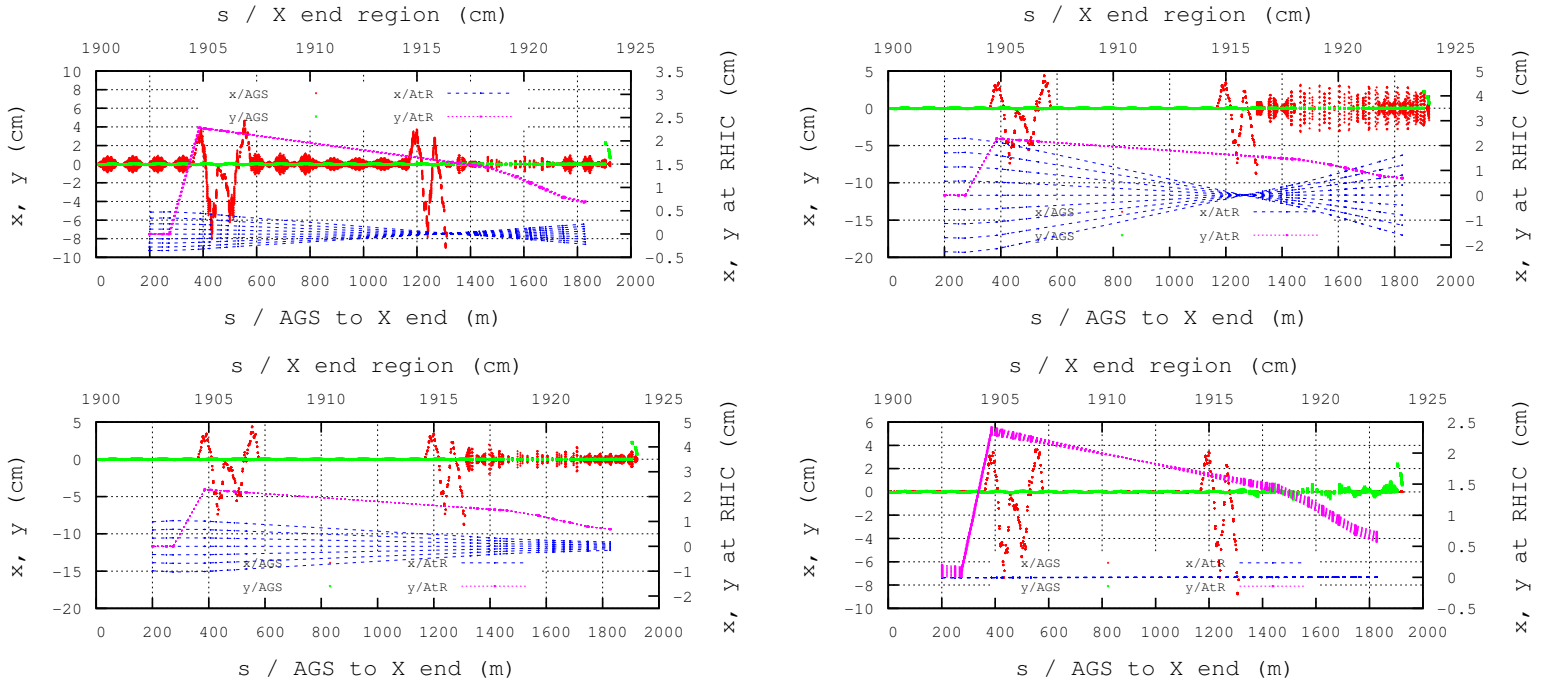

Figure 12: Top left : chromatic orbits along AGS and down to X end (red and green curves, bottom horizontal and left vertical scales) and at the end of X line (top horizontal and right vertical scales), over the $\delta p/p$ range explored. Other three plots : perturbed orbits along AtR due to x_0- (top right) or x'_0- (bottom left) or y_0-perturbation (bottom right) at start of AtR line.

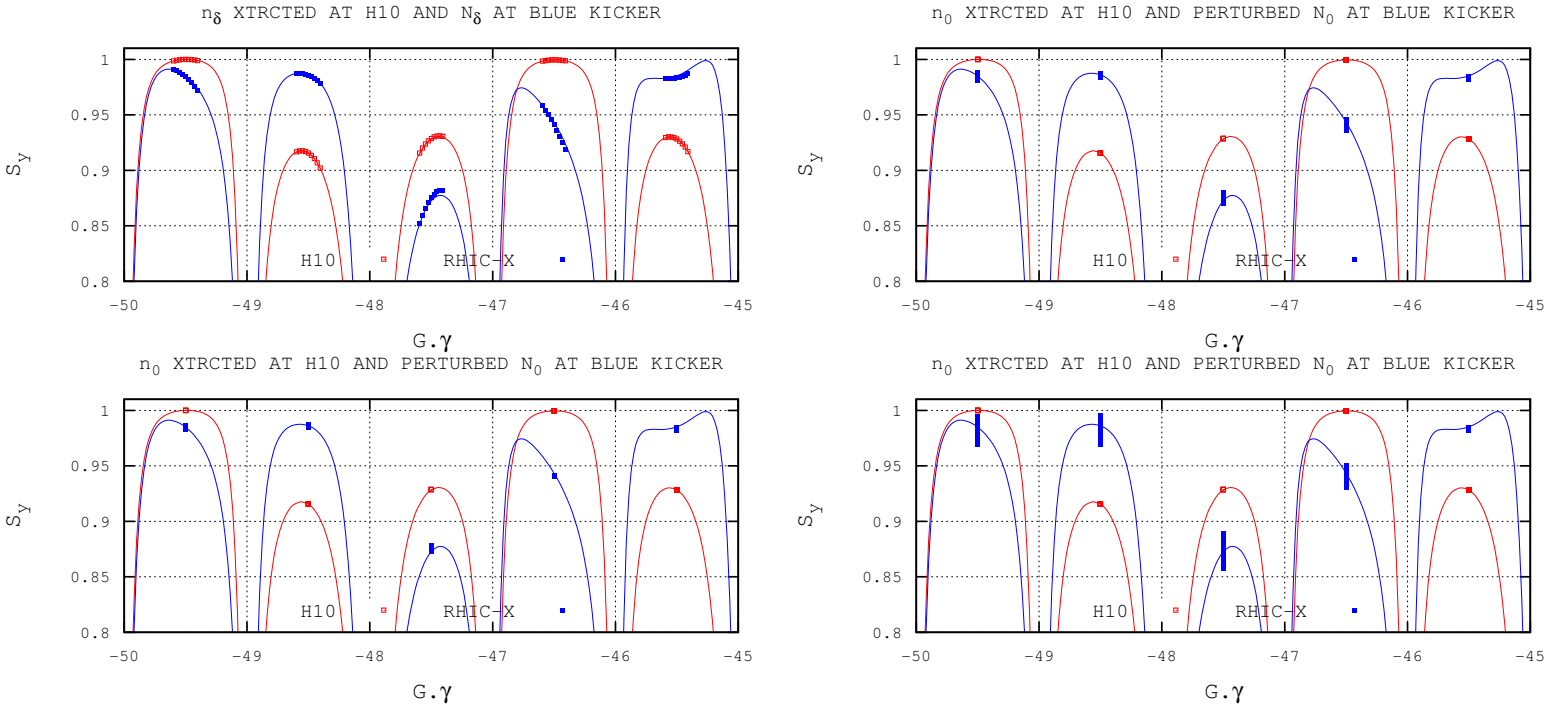

Figure 13: Top left : Vertical component of the chromatic spin vector $\vec{n}_\delta$ at extraction from AGS (at H10 septum, red squares), and at RHIC Blue injection kicker (blue squares). Other three plots : S_y at extraction from AGS (unperturbed by hypothesis, red squares), and at RHIC Blue injection kicker (blue squares), in case of x- (top right), x'- (bottom left) or y-perturbation (bottom right) at start of AtR line. The unperturbed case vertical component $\vec{n}_0$ (as displayed in Fig. 11) is reproduced here for comparison (solid lines).

This sequence is repeated for five different 500-particle bunches with respective rms Gaussian widths $\epsilon_y/\pi = 0,\ 2.5,\ 5,\ 10\,\mu$m, normalized.

The results are displayed in Fig. 14, a zoom on the central part ($G\gamma \in [-50, -45]$) is given in Fig. 15. The effect of vertical emittance is apparent : depending on $G\gamma$, $< S_y >$ varies by up to several % (absolute) for $\epsilon_y\ : 0 \rightarrow 4\epsilon_{y,\,rms}$.

In order to illustrate the behavior of the bunch, Fig. 16 shows the vertical coordinates of 100 particles along the optical elements in the AGS and down to RHIC Blue kicker, in the case of the rms value $\epsilon_y/\pi = 2.5\,\mu$m normalized (truncated at $9\sigma_{\epsilon_y}$) - it can be verified that this beam bundle follows the beam envelopes along the U-W-X line as shown in Fig. 10.

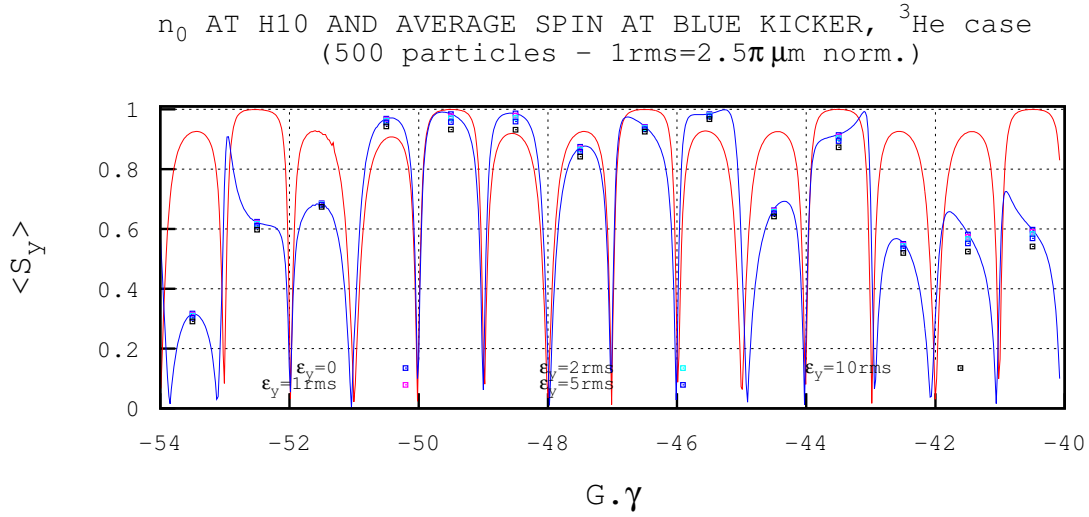

Figure 14: Effect of non-zero vertical emittance. Markers : average value of the vertical component of the spin vector at RHIC Blue injection kicker in the case of 500 random particles in Gaussian beam emittance with vertical emittance either $0,\ 1,\ 2,\ 5,$ or 10 times the regular rms beam emittance, truncated at $9\sigma_{\epsilon_y}$ (rms $\epsilon_y = 2.5\,\pi\mu$m, normalized). Solid lines are in the zero-emittance case (as in Fig. 11), for comparison : the red one is at H10, the blue one is at RHIC.

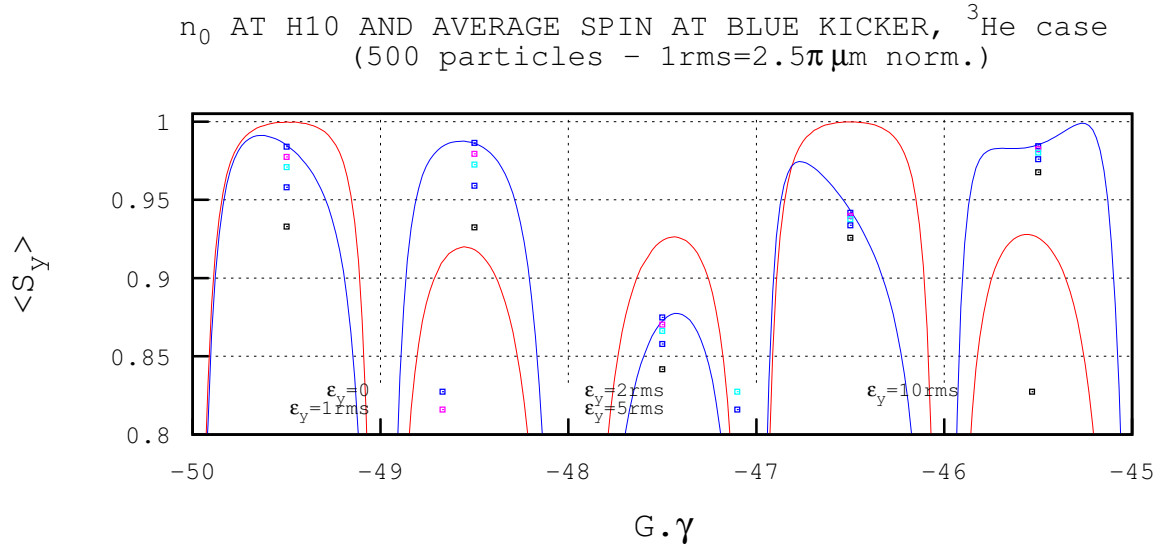

Figure 15: Effect of non-zero vertical emittance. This is a zoom on the central region of Fig. 14. $\epsilon_y = 0$ straddles the solid line, $\epsilon_y = 10\ rms$ ($\approx 25\pi\mu$m) is the lowest, black marker.

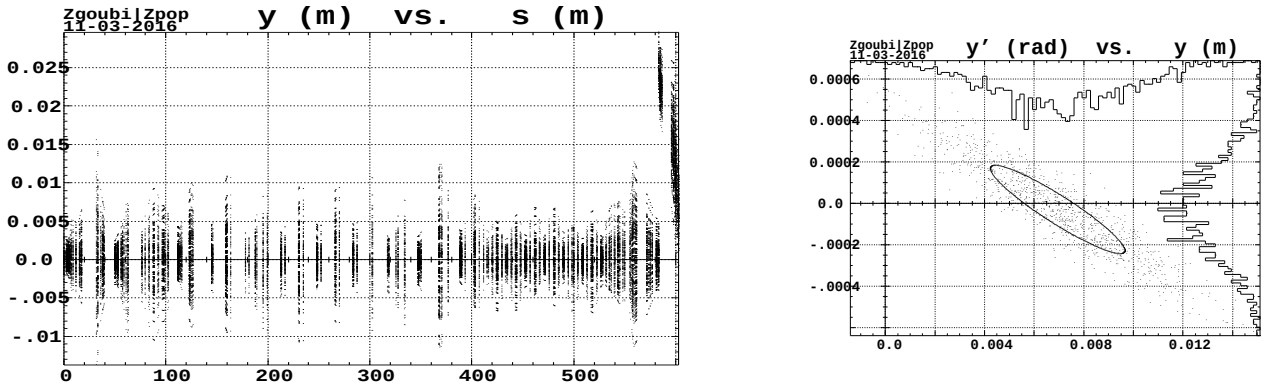

Figure 16: Left : sample beam bundle (100 particles, vertical excursion) as tracked in Zgoubi, from UBegin down to RHIC Blue kicker, in the case $\epsilon_y/\pi = 2.5\,\mu$m norm. (truncated at $9\sigma_{\epsilon_y}$). Note that the bundle is vertically off-centered at the downstream end of the line, this is when Zgoubi reference frame along AtR is moved up by 2.5 cm at entrance to RHIC QFB6 quadrupole. Right : particle bunch in vertical phase space as it arrives at RHIC kicker, and the rms matching invariant (ellipse), which is measured to be $0.21\,\mu$m non normalized as expected ($\sim 2.5\,\mu$m, normalized).

APPENDIX

A AGS optics in Zgoubi for $\vec{n}_0$ search

A.1 Orbit

Below are given the status of the variables (namely, fields in F, G, H, I dipoles of concern) and of the constraints (orbit position and angle at various s-locations) at completion of the G09 and H11 bumps optimization, showing that the double-bump is well closed.

H and V orbits are displayed in Fig. 6, the non-fully zero excursion is due to the snakes.

```
STATUS OF VARIABLES  (Iteration #     0 /     90 max.)
 LMNT  VAR  PARAM   MINIMUM     INITIAL         FINAL          MAXIMUM     STEP     NAME      LBL1     LBL2
  454    1     13   -1.00       5.282E-02   5.2823394243E-02   1.00      2.743E-05 AGSMM     MM_F08CD   *
  460    2     13   -1.00       2.107E-02   2.1067544000E-02   1.00      2.743E-05 AGSMM     MM_F09BF   *
  505    3     13   -1.00      -4.765E-02  -4.7651905840E-02   1.00      2.743E-05 AGSMM     MM_G02BF   *
  511    4     13   -1.00      -2.188E-02  -2.1876893000E-02   1.00      2.743E-05 AGSMM     MM_G03CD   *
  563    5     13   -1.00      -0.227      -0.2274574949       1.00      2.743E-05 AGSMM     MM_G16AD   *
  565    6     13   -1.00       5.382E-03   5.3820169679E-03   1.00      2.743E-05 AGSMM     MM_G17CF   *
  596    7     13   -1.00      -4.071E-02  -4.0708518000E-02   1.00      2.743E-05 AGSMM     MM_H04CD   *
  600    8     13   -1.00      -7.091E-02  -7.0914279000E-02   1.00      2.743E-05 AGSMM     MM_H05AF   *
  655    9     13   -1.00      -0.327      -0.3267328624       1.00      2.743E-05 AGSMM     MM_H18CF   *
  661   10     13   -1.00       0.452       0.4518542586       1.00      2.743E-05 AGSMM     MM_H19BD   *
  705   11     13   -1.00      -7.574E-03  -7.5744321350E-03   1.00      2.743E-05 AGSMM     MM_I12BD   *
  711   12     13   -1.00       8.204E-02   8.2041498222E-02   1.00      2.743E-05 AGSMM     MM_I13CF   *
STATUS OF CONSTRAINTS (Target penalty =   1.0000E-02)
TYPE  I   J  LMNT#       DESIRED          WEIGHT          REACHED          KI2       NAME      LBL1     LBL2          *
  3   1   2   476      3.2528130E+00     1.0000E+00    3.1032372E+00   7.8343E-03   DRIFT     DSS        F14CF_up    *
  3   1   2   487      3.3242720E+00     1.0000E+00    3.4252566E+00   3.5710E-03   DRIFT     DSQ        QH_F17_up   *
  3   1   2   540     -6.1000000E+00     1.0000E-01   -6.1006362E+00   1.4174E-05   MARKER    G10MID     *           *
  3   1   3   540      6.1000000E+00     2.0000E+00    5.5390824E+00   2.7543E-02   MARKER    G10MID     *           *
  3   1   2   624     -7.0120130E+00     1.0000E+00   -5.5867029E+00   7.1137E-01   DRIFT     D2SH       H10BF_up    *
  3   1   2   627     -4.8000000E+00     1.0000E-01   -4.8242132E+00   2.0530E-02   MARKER    H10MID     MARK        *
  3   1   3   627      4.8000000E+00     2.0000E+00    3.6866999E+00   1.0850E-01   MARKER    H10MID     MARK        *
  3   1   2   638     -5.5000000E+00     1.0000E+00   -4.9207377E+00   1.1750E-01   DRIFT     DSS        SXH_H13_up  *
  3   1   2   684      4.3165590E+00     1.0000E+00    4.3501333E+00   3.9472E-04   DRIFT     DRIF       D2H_MID     *
  3   1   2   693      3.2571530E+00     1.0000E+00    3.1686097E+00   2.7453E-03   DRIFT     DRIF       I08_up      *
  3   1   2   712      0.0000000E+00     2.0000E+01    1.5830217E-02   2.1938E-07   DRIFT     DSS        SXH_I13_up  *
```

```
   3   1   3   712      0.0000000E+00     2.0000E+01    2.7421308E-03   6.5825E-09   DRIFT      DSS        SXH_I13_up *
 Fit reached penalty value   2.8558E+00
```

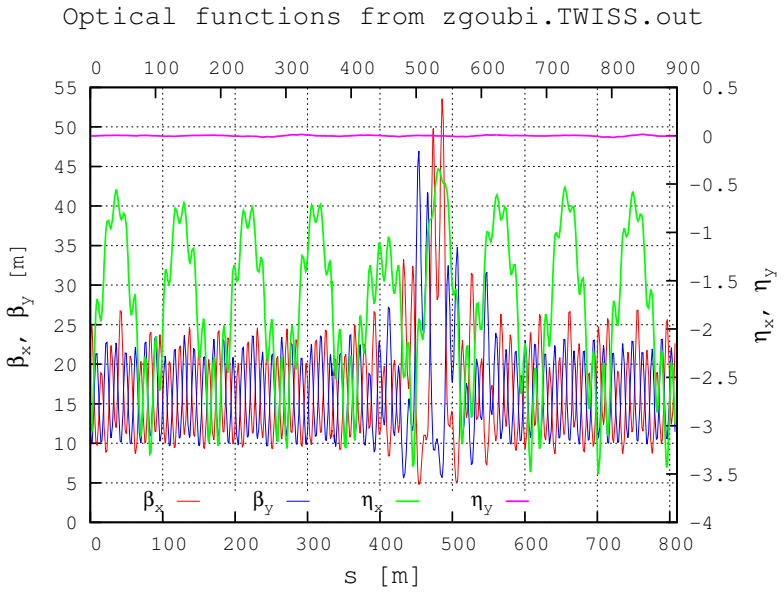

Figure 17: Optical functions in Zgoubi for $\vec{n}_0$ search and $G\gamma$ scans. η_x, η_y, right scale, are the periodic dispersion functions.

A.2 Betatron functions

The optical functions in the AGS are shown in Fig. 17. They can be considered stable during the $G\gamma$ scan (what changes depending on particle momentum is the main magnet focusing and the optical strength of the snakes as they are operated at constant field, however these are small effects).

B Zgoubi input data file for $\vec{n}_0$ scan at H10

Below is given an excerpt of zgoubi.dat input data file, including "FIT" and its appropriate arguments, as used for finding the stable spin vector $\vec{n}_0$ at A01BF in the AGS, and, following that, transporting it to UBegin, where a 500-particle Monte Carlo object is fabricated ('MCOBJET', right column), with all spins aligned on $\vec{n}_0$ at UBegin. The snakes are shown explicitly for clarity (maps used, settings, etc.).

The final "SYSTEM" command in the data list (bottom of the right column) stores the orbits and their $\vec{n}_0$ in a dedicated file, "catOrbits.data", for possible further plotting.

A complete zgoubi.dat file is available in the AGS Zgoubi model development area, namely

$$/rap/lattice\_tools/zgoubi/AgsZgoubiModel/AtR/3He/n0$$

```
Template zgoubi.dat. 2 snakes.
 'OBJET'     LBL_OBJfit
----BORO_ref----
2
1 1
 3.1423E-04 -5.4803E-03 -5.5249E-03 -3.2524E-02 0.00  1.0 'o'
1
 'PARTICUL'
2808.39148  3.204352974e-19  -4.18415382  0. 0.

 'SPNTRK'
4.1
SX SY SZ ! spin comp

 'GETFITVAL'
fitVals_G09H11.data

 'SCALING'   LBL_SCLfit
1   10
AGSMM *AF *BF *CF  ! dB0 (FIT#3),  dB1 (FIT#4),  dB2
-1         3        13   1.       14    4e-20   15   5.E-20
1.000000006    ! (FIT #6)
1
AGSMM *AD *BD *CD  ! dB0 (FIT#9),  dB1 (FIT#10), dB2
-1         3        13   1.       14   10e-20   15   11.E-20
1.00000012    ! (FIT#12)
1
AGSQUAD
-1
0.
1
AGSQUAD
-1
0.
1
MULTIPOL
-1
----BORO_ref_Tm----
1
MULTIPOL HKICE VKICE
-1
0.
1.
MULTIPOL SMG10 Septum h11bd h12bd h13cf
-1
----BORO_ref_Tm----
1
MULTIPOL AtR
-1
----DRef----
1
MULTIPOL RHIC RHICQ
-1
----BORO_ref_Tm----
1
BEND RHICB
-1
----BORO_ref_Tm----
1

 'MARKER'   #Start

'OPTIONS'
 1  1
 WRITE ON

'AGSMM'  MM_A01BF
.................................
... DOWN TO THE COLD SNAKE    ....
.................................
'TOSCA'
0  0
10. 1. 1. 1.
HEADER_9
321 29 29  15.2  0.76015  0.228
b_ags-full-coilv5-x06-rerun2-x071-integral-x5y5z10mm.table
b_ags-full-sold3-only-nodal-x5y5z10mm-wasActually-integral.table
0 0 0 0
2
.1
2  0.  1.390582384  0.  0.
.................................
... DOWN TO THE WARM SNAKE    ....
.................................
 'TOSCA'
0  0        1.e1   100. 100. 100.
HEADER_0 wsnake
801 29 29 15.1 1.
Wsnk3D_map/b_table55.TAB
0 0 0 0
2
.1
2  0.  .00  0.  0.
.................................
... THE REST OF THE AGS RING  ....
.................................
'AGSMM'  MM_L20BD
0
   3.000000   0.00   0.00  0.00000000E+00  0.10000000E+01  0.10000000E+01
2  1 0.  1 0.
0. 0. 10.00  4.0  0.800 0.00 0.00 0.00 0.00 0. 0. 0. 0.
4  .1455   2.2670  -.6395  1.1558  0. 0.  0.
0. 0. 10.00  4.0  0.800 0.00 0.00 0.00 0.00 0. 0. 0. 0.
4  .1455   2.2670  -.6395  1.1558  0. 0.  0.
0. 0. 0. 0. 0. 0. 0. 0. 0. 0.
10.0  Dip MM_L20BD
3    0.0000000   -0.3917463    0.011751150  angle =  -0.02350230 rad
'DRIFT' DRIF D10
152.3839
'DRIFT' DRIF D10
152.3839
 'MARKER'   #End
 'FIT'
7   nofinal save
1  30  0  [-1., +1.]
1  31  0  [-1., +1.]
1  32  0  [-1., +1.]
1  33  0  [-1., +1.]
3  10  0  [-1., +1.]
3  11  0  [-1., +1.]
3  12  0  [-1., +1.]
8    1.0000E-8   1000
 3.1 1 2  #End 0. 1.  0
 3.1 1 3  #End 0. 1.  0
 3.1 1 4  #End 0. 1.  0
 3.1 1 5  #End 0. 1.  0
10.1 1 1 #End 0. 1.  0
10.1 1 2 #End 0. 1.  0
10.1 1 3 #End 0. 1.  0
10   1 4 #End 1. .01 0

 'GETFITVAL'
fitVals_G09H11Bumps.data
'MARKER'   #Start
'AGSMM'  MM_A01BF
.....................................
... AGS RING SEQUENCE DOWN TO UBegin  ....
.....................................
 'SPNPRT'

 'SYSTEM'   ! This allows saving local n_0 for further use by SPNTRK, below
grep -n1 "       (deg)" zgoubi.res > spin.data

 'MCOBJET'     LBL_OBJfit
----BORO_ref----
3
500                       ! Number of particles in bunch
2 2 2 2  2  2
0. 0. 1.e-5 1.e-5 0. 1.
-4.1 37.5  0.  9.          ! alpha_x, beta_x
.850 6.5   2.e-7  9.       ! alpha_x, beta_x, epsilon_y/pi
0. 1. 0.  4
123456 234567 345678

 'PARTICUL'
2808.39148  3.204352974e-19  -4.18415382  0. 0.

 'SPNTRK'
4.2
spin.data

 'CHANGREF'
 ZS 0. ZR 0.    !!  y and yp co
 'MARKER'   MARK      UBEGIN
.............................
... The rest of the AtR ......
.............................
 'MULTIPOL'  RHIC VKIC    INJKICKR
0  .kicker
100. 10.00   -0.02   0.000000 0.0 0.0 0.0 0.0 0.0 0.0 0.0 0.0
.0 .0  1.00 0.00 0.00 0.00 0.00 0. 0. 0. 0.
6 .015527 3.874961 -2.362230 2.978209 12.604429 15.025689
.0 .0  1.00 0.00 0.00 0.00 0.00 0. 0. 0. 0.
6 .015527 3.874961 -2.362230 2.978209 12.604429 15.025689
1.570796327 0. 0. 0. 0. 0. 0. 0. 0. 0.
#20|20|20  Kick
1 0. 0. 0.

 'SPNPRT' PRINT

 'SYSTEM'   ! This allows checking the bumps in the whole Ggamma scanned range.
2
cat zgoubi.fai >> catOrbits.data
cat zgoubi.FITVALS.out >> catFitVals.data

 'END'
```

References

[1] Where are the AGS snakes ?, F. Méot, R. Gupta, H. Huang, N. Tsoupas, Tech. Note C-A/AP/485, July 2013.

[2] On the image in RHIC of AGS $\vec{n}_0$, via the AtR, F. Méot, H. Huang, N. Tsoupas, Tech. Note C-A/AP/502, July 2013.

[3] Spin transport from AGS to RHIC with two partial snakes in AGS, W. MacKay et al., Procs. EPAC 2006 Acc. Conf., Edinburgh.

[4] Closed orbit calculations at AGS and extraction beam parameters at H13, N. Tsoupas et al., Tech Note AD/RHIC/RD-75, Oct. 1994.

[5] Stable spin direction of a polarized proton beam at the injection point of RHIC, N. Tsoupas et al., Spin Note AGS/RHIC/SN 021, March 1996.

[6] The ray-tracing code Zgoubi, http://sourceforge.net/projects/zgoubi/
Zgoubi Users' Guide, F. Méot, Report CA/AP/470, BNL C-AD, Oct. 2012.

[7] Development of a stepwise ray-tracing based on-line model at AGS, F. Méot et al., Procs. PAC 2011 Acc. Conf., NY.
Modelling of the AGS using Zgoubi - status, F. Méot et al., Procs. IPAC 2011 Acc. Conf., San Sebastian.

[8] Helical dipole partial snakes for the AGS, J. Takano et al., JINST1, P11002 (2006).